Numerical Analysis of LNG as a Coolant in Liquid Rocket Engines

A. Urbano⋆ and F. Nasuti⋆⋆
⋆Ph.D. student,e-mail: annafederica.urbano@uniroma1.it
⋆⋆Associate Professor, AIAA Senior Member, e-mail: francesco.nasuti@uniroma1.it
University of Rome "La Sapienza", Roma, Italy
Dipartimento di Ingegneria Meccanica e Aerospaziale, Via Eudossiana 18, Roma 00184, Italy

1. Introduction

Liquid Natural Gas (LNG) is a suitable propellant to be used, together with liquid oxygen as an oxidizer, in a liquid rocket engine because of possible advantages with respect to hydrogen in specific applications. In the design phase of a regenerative cooled liquid rocket engine, the knowledge of the different thermodynamic phenomena that could affect the propellant flow in the cooling channels is fundamental. This is especially important in the case of an expander cycle for which the performance is strictly connected with the heat transfer characteristics in the cooling channels. Depending on the engine design, LNG used as a coolant can flow in those channels at supercritical pressures and in the neighborhood of the critical point. In such conditions the strong properties variations could change the heat transfer capabilities of the propellant by either a heat flux deterioration or enhancement. The main goal of the present work is to investigate the effect of the parameters that could affect the heat transfer characteristics of LNG. To pursue this objective a fast and suitable numerical solver is essential. While the motivation for choosing a fast solver in a parametric study is obvious, a suitable solver is necessary to manage the complex flow modeling and thermodynamic phenomena, which affect heat transfer to turbulent supercritical fluids. The proposed approximation is to use parabolized Navier-Stokes equations[1, 2]. Parabolization is obtained by neglecting viscous derivatives in the space-marching direction and by considering the streamwise pressure gradient as a source term evaluated on the basis of the overall momentum balance. The main advantage in using a PNS solver is a substantial saving of computational time with respect to a full Navier-Stokes solver, with a reasonably small loss in accuracy. The algorithm is based on a finite volume approach, which uses a modified Roe's approximate Riemann solver for a fluid governed by a generic equation of state (EOS). To this end a mixing rule is necessary to describe the thermodynamic properties of LNG which is essentially a mixture of more than 90% methane and other heavier hydrocarbons in minor quantities. The GERG [3] model has been selected for the EOS, whereas the Extended Corresponding States (ECS) models of Huber and Klein [4, 5] have been used for the transport properties. In the following an introduction of the work is presented: first the parabolized Navier-Stokes equations are recalled together with the principal features of the numerical model implemented to solve them, and a brief description of the mixture EOS and transport properties. Then the results of the PNS solver validation are reported and commented: it is a comparison between numerical results and experimental data. The selected test case is particularly interesting because it is a turbulent heated flow of transcritical hydrogen that exhibits a deterioration in the heat transfer. Then, as an example of the test cases that will be analyzed in the final paper, a heated flow of supercritical methane is presented. In the final paper a parametric study will be presented: the aim is to investigate on the influence of different parameters, like operating pressure, temperature, mass flow rate and heat flux, on the heat transfer and flow field. Finally attention will be devoted to the differences in the heat transfer characteristics varying the percentage of methane in the LNG mixture, from 90% to 100% (pure methane).

2. Governing Equations

The parabolization of Navier-Stokes equations is obtained considering that a channel flow has a predominant flow direction. On this basis, the following assumptions can be made:

- the derivatives in the streamwise direction in the diffusive terms are of lower order of magnitude than the same derivatives in the transverse directions;
- the velocity in the streamwise direction is always positive: no reverse flow occurs;
- the pressure gradient in the streamwise direction is constant along each transverse plane.

Under these assumptions a fully parabolized form of the steady Navier-Stokes equations can be considered to describe the flow behavior. Considering a Cartesian reference system for a straight tube, if x is the streamwise direction and y,z are the transverse directions, the conservative form of the three-dimensional PNS equations is:

$$\frac{\partial \mathbf{F_e}}{\partial x} + \frac{\partial \mathbf{G_e}}{\partial y} - \frac{\partial \mathbf{G_v}}{\partial y} + \frac{\partial \mathbf{H_e}}{\partial z} - \frac{\partial \mathbf{H_v}}{\partial z} = \mathbf{Q} \tag{1}$$

where the subscripts $()_e$ and $()_v$ indicate the Eulerian and viscous flux vectors, respectively, after the PNS approximations have been applied. These equations have been obtained by neglecting the streamwise viscous flux vector and the x derivatives in the transverse viscous flux vectors (in $\mathbf{G_v}$ and $\mathbf{H_v}$ all the x derivatives have been neglected). A source term vector $\mathbf{Q}$ has been emphasized in Eq. (1) for the sake of generality. The resulting expressions of the flux vectors are:

$$\mathbf{F_e} = \begin{Bmatrix} \rho u \\ \rho u^2 + p \\ \rho uv \\ \rho uw \\ \rho u h_0 \end{Bmatrix} \qquad \mathbf{G_e} = \begin{Bmatrix} \rho v \\ \rho uv \\ \rho v^2 + p \\ \rho vw \\ \rho v h_0 \end{Bmatrix} \qquad \mathbf{H_e} = \begin{Bmatrix} \rho w \\ \rho uw \\ \rho vw \\ \rho w^2 + p \\ \rho w h_0 \end{Bmatrix} \tag{2}$$

$$\mathbf{G_v} = \begin{Bmatrix} 0 \\ \mu \dfrac{\partial u}{\partial y} \\ \dfrac{3}{2}\mu\left(2\dfrac{\partial v}{\partial y} - \dfrac{\partial w}{\partial z}\right) \\ \mu\left(\dfrac{\partial v}{\partial z} + \dfrac{\partial w}{\partial y}\right) \\ uG_{v,2} + vG_{v,3} + wG_{v,4} + k\dfrac{\partial T}{\partial y} \end{Bmatrix} \qquad \mathbf{H_v} = \begin{Bmatrix} 0 \\ \mu \dfrac{\partial u}{\partial z} \\ \mu\left(\dfrac{\partial v}{\partial z} + \dfrac{\partial w}{\partial y}\right) \\ \dfrac{3}{2}\mu\left(2\dfrac{\partial w}{\partial z} - \dfrac{\partial v}{\partial y}\right) \\ uH_{v,2} + vH_{v,3} + wH_{v,4} + k\dfrac{\partial T}{\partial z} \end{Bmatrix} \tag{3}$$

where subscripts $()_2$, $()_3$, $()_4$, indicate the second, third and fourth component of vectors, respectively. The system of equations (1) is a parabolic system only if the flow is supersonic in the streamwise direction, whereas the pressure gradient in the x direction permits information to be propagated upstream in case of subsonic flow: in the latter case from a mathematical point of view the system is elliptic. The influence of the streamwise pressure gradient term on the mathematical nature of the PNS equations has been studied by Vigneron et al. [6] who showed that if only a fraction ω ($0 \leq \omega \leq 1$) of the streamwise pressure gradient (dp/dx) is retained in the equations, the system becomes parabolic also in the case of subsonic flow. The value of the parameter ω which makes the system parabolic depends on the local flow Mach number. Nevertheless, the system is always parabolic if ω is set to 0, that is if the streamwise pressure gradient is no longer considered as an unknown. In this case the equation system is recasted as:

$$\frac{\partial \overline{\mathbf{F}}_\mathbf{e}}{\partial x} + \frac{\partial \mathbf{G_e}}{\partial y} - \frac{\partial \mathbf{G_v}}{\partial y} + \frac{\partial \mathbf{H_e}}{\partial z} - \frac{\partial \mathbf{H_v}}{\partial z} = \frac{\partial \mathbf{P}}{\partial x} + \mathbf{Q} \tag{4}$$

where pressure gradient has been moved to right hand side to emphasize that it is considered as a source term of the parabolic system. The new symbols introduced with respect to Eq. (1) are:

$$\overline{\mathbf{F}}_\mathbf{e} = \begin{Bmatrix} \rho u \\ \rho u^2 \\ \rho uv \\ \rho uw \\ \rho u h_0 \end{Bmatrix} \qquad \mathbf{P} = \begin{Bmatrix} 0 \\ -p \\ 0 \\ 0 \\ 0 \end{Bmatrix} \tag{5}$$

The streamwise pressure gradient is considered as a source term **P** which is either known a priori or evaluated on the basis of integral cross section balances, as will be discussed in the following.
An eddy viscosity approach has been considered for the turbulence with the one equation model of Spalart Allmaras [7] modified to take into account the PNS hypothesis. The diffusion-convection equation for the turbulent viscosity is solved together with Eqs. 4, in which the turbulent viscosity and conductivity are added to the molecular values.

3. Numerical Model

The numerical solution of Eq. (4), in which the streamwise pressure gradient is treated as a source term, is carried out considering that the system of equations is parabolic in the streamwise direction and elliptic in the transverse directions: the equations can be therefore solved using a space-marching method. The present space-marching method relies on a finite volume scheme in which the unknown $\overline{\mathbf{F}}_\mathbf{e}$ fluxes are integrated in the x direction with an Euler explicit scheme once the $\mathbf{G}_e$, $\mathbf{G}_v$, $\mathbf{H}_e$, and $\mathbf{H}_v$ fluxes have been evaluated at the cell interfaces. Following this approach, and referring to the generic integration cell (i, j, k) of Fig. 1, Eq. (4) can be written as:

$$\overline{F}_{e,i+1} = \overline{F}_{e,i} - \frac{1}{\mathcal{A}_{x,i}} \int_{\mathcal{S}_{l,i}} (\mathbf{G}_e n_y - \mathbf{G}_v n_y + \mathbf{H}_e n_z - \mathbf{H}_v n_z) d\mathcal{S} + Q\Delta x + \Delta P \tag{6}$$

where $\Delta x = x_{i+1} - x_i$ and $\Delta P = P_{i+1} - P_i$ and n_y, n_z are the components in the y and z directions, respectively, of the outward unit vector normal to the longitudinal surface of the integration cell. The $\overline{F}_{e,i}$ fluxes are considered constant over the single transverse cell-face surface of area $\mathcal{A}_{x,i}$, which provides the first order of the scheme. The viscous fluxes $\mathbf{G}_v$ and $\mathbf{H}_v$ are computed with central differences, whereas the Eulerian fluxes $\mathbf{G}_e$ and $\mathbf{H}_e$ at each cell interface are obtained as the solutions of a Riemann problem. The Riemann solver is a modified version of the Roe's approximate Riemann solver[8] for Eq. (4) with generic equations of state:

$$h = h(p, \rho)\,; \qquad T = T(p, \rho)\ \ldots \tag{7}$$

with h enthalpy, T temperature, p pressure and ρ density. A *CFL* condition permits, once all the eigenvalues have been evaluated, to choose a Δx integration step which provides a stable scheme.

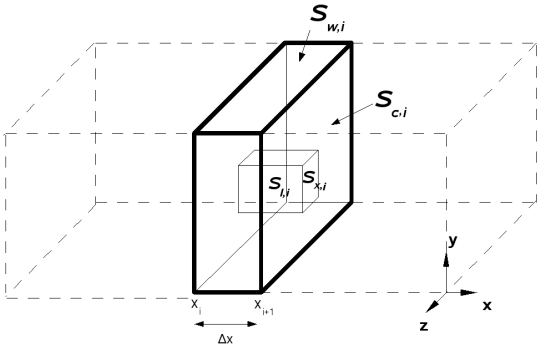

Figure 1: Schematic of a generic 3D control volume

3.1 Streamwise pressure gradient

One of the critical points of the algorithm is how to compute the streamwise pressure gradient, which has to be evaluated at each integration step. The **P** term in Eq. (4) is evaluated with an iteration process, imposing the conservation of the integral momentum equation for each step of channel of length Δx. Referring to Fig. 1 the pressure variation has to verify the following balance equation:

$$\int_{\mathcal{S}_{c,i+1}} (\rho u^2 + p) dS = \int_{\mathcal{S}_{c,i}} (\rho u^2 + p) dS - \int_{\mathcal{S}_{w,i}} \mu \frac{\partial u}{\partial n} d\mathcal{S} \tag{8}$$

in which $\mathcal{S}_{c,i+1}$ indicates the channel cross section surface, and $\mathcal{S}_{w,i}$ the wall surface of channel in the length Δx. For example, for a 2D planar channel Eq. (8) becomes:

$$\frac{d}{dx}\left(\int_0^H (\rho u^2 + p)dy\right) - \left(\mu\frac{\partial u}{\partial y}\bigg|_H - \mu\frac{\partial u}{\partial y}\bigg|_0\right) = 0 \tag{9}$$

where H is the height of the channel. It is assumed that the pressure gradient in the streamwise direction does not depend on the transverse position in the transverse plane.

4. Mixture Models

4.1 Equation of State

Dealing with LNG, which is a mixture of more than 90% methane and other heavier hydrocarbons in minor quantities, the most recent and reliable equations of state are those presented in the GERG study [3]. They are based on the Helmholtz free energy, which takes into account the real behavior of fluids with some kind of departure functions from the perfect gas solution. In particular, the GERG EOS is based on pure substances equations of state for each considered mixture component and correlation equations for binary mixtures consisting of these components. Mixing rules are applied to the reduced Helmholtz free energy a:

$$a(\delta, \tau, \overline{x}) = \frac{A}{RT} = a^0(\rho, T, \overline{x}) + a^r(\delta, \tau, \overline{x}) \tag{10}$$

with ρ and T being respectively the mixture density and temperature, R the gas constant, A the mass specific Helmholtz free energy, and $\overline{x} = (x_1, x_2, \ldots, x_N)$ the molar composition. The residual term a^r, which corrects in the real fluid regime the perfect gas term a^0, is expressed in terms of reduced mixture density δ and reduced mixture temperature τ, according to:

$$\delta = \frac{\rho}{\rho_r(\overline{x})} \qquad \text{and} \qquad \tau = \frac{T_r(\overline{x})}{T} \tag{11}$$

The equation of state describing the Helmholtz free energy as a function of temperature and density, with its derivatives, is sufficient to provide a complete description of the thermodynamic properties of the mixture and is sometimes termed the “fundamental equation”. Once the equation of state for the reduced Helmholtz free energy is available, the other thermodynamic properties of the mixture (compressibility factor, pressure, enthalpy, specific heats...) can be obtained from its derivatives with respect to reduced temperature and density.

4.2 Transport properties

In the field of real fluid the most commonly used approach followed in the literature to get mixture viscosity and thermal conductivity is ECS theory. In the present study, transport properties have been evaluated according to ECS theory presented in [4, 5]. In this theory viscosity and thermal conductivity are accurately evaluated for a reference fluid (R134a) whose properties are taken from [4, 9]. In general the viscosity of the fluid mixture will be expressed (according to [10]) as:

$$\mu = \mu^0(T, \overline{x}) + \mu^r(T, \rho, \overline{x}) + \mu^m(T, \rho, \overline{x}) \tag{12}$$

where μ^0 is the diluted gas term, μ^r is the residual viscosity, and μ^m is a correction term for mixtures. The latter term will be neglected in the present study as is usually done for many of the fluid conditions of interest. The basic assumption of the ECS model is that:

$$\mu^r(T, \rho, \overline{x}) = \mu_0^r(T_0, \rho_0)F_\mu^r \tag{13}$$

namely, the residual viscosity of the mixture is equal to the residual viscosity of the reference fluid μ_0^r evaluated at the conformal temperature T_0 and density ρ_0 and modified for a correction factor F_μ^r. Assuming that the residual viscosity of the reference fluid as a function of temperature and density is known, it is only necessary to evaluate conformal temperature and density and the reducing factor F_μ^r. The conformal temperature and density are defined as such that:

$$\begin{cases} a^r(T, \rho, \overline{x}) = a_0^r(T_0, \rho_0) \\ \\ Z(T, \rho, \overline{x}) = Z_0(T_0, \rho_0) \end{cases} \tag{14}$$

where a^r is the residual part of the reduced Helmholtz free energy ($a = A/RT$) and Z the compressibility factor of the mixture, whereas a_0^r and Z_0 are the corresponding functions for the reference fluid.

The evaluation of thermal conductivity follows the same procedure as for viscosity. In general the thermal conductivity of the fluid mixture will be expressed (according to [11]) as:

$$k = k^0(T, \overline{x}) + k^r(T, \rho, \overline{x}) + k^c(T, \rho, \overline{x}) \tag{15}$$

where k^0 is the diluted gas term, k^r is the residual viscosity, and k^c is the so-called critical enhancement which allows to predict the thermal conductivity peak in the vicinity of the critical point. The basic assumption of the ECS model is as in case of viscosity:

$$k^r(T, \rho, \overline{x}) = k_0^r(T_0, \rho_0) F_k^r \tag{16}$$

namely, the residual thermal conductivity of the mixture is equal to the residual thermal conductivity of the reference fluid k_0^r evaluated at the conformal temperature T_0 and density ρ_0 and modified for a correction factor F_k^r.

5. Validation: comparison with experimental data

The present PNS solver has been validated in [2] by the study of a test case for which experimental data are available in the open literature. In particular, the selected test case is one of those presented in [12], which is a detailed experimental study of hydrogen flow in heated tubes at sub- and super-critical pressures. Among all the test cases, the "64_706" has been selected because of the particular thermodynamic condition of the hydrogen which can be of great interest in the field of rocket cooling channels. Test case inlet and exit temperature are 25 and 53 K, respectively, and the inlet pressure is 5 MPa. Consequently hydrogen operative condition is transcritical: in fact the pressure is supercritical ($p/p_c \simeq 3.8$) and the inlet temperature is subcritical ($T/T_c \simeq 0.8$) while the exit temperature is supercritical ($T/T_c \simeq 1.8$).

This test case is of particular interest because it presents heat transfer deterioration. This phenomenon can appear in the case of supercritical pressure fluids with pressure and temperature close to the critical ones (near critical fluids). In fact, if such a fluid is heated up in a channel and passes from a temperature smaller than the pseudocritical temperature T_{ps} to a temperature greater than T_{ps}, a pseudo phase-change occurs[13, 14] (the pseudo-critical temperature is the temperature at which specific heat at constant pressure has a maximum at a specified pressure). The fluid passes from a liquid-like to a gas-like state with an abrupt change in all the properties[15]. This can lead to a deterioration of the heat transfer at low mass flow rate, high heat flux and fluid and wall temperature being, respectively, lower and higher than the pseudo-critical value[16, 17, 18, 19]. In fact, due to the large heat flux, along the tube the temperature near the wall increases and exceeds the pseudocritical one. As a consequence the density undergoes an abrupt fall: a gaseous film appears near the wall, characterized by a low thermal capacity and a low density. This brings to a deterioration of the heat transfer and thus ton a great increase in the wall temperature. More downstream also the bulk temperature reaches the pseudocritical value leading to an increase in the velocity and thus in the heat transfer: as a result the wall temperature decreases. As a matter of fact if the deterioration occurs, the wall temperature first grows and then decreases, that is it shows a peak.

The mass flow rate per unit area of the tube cross section is 1324 $\mathrm{kg/m^2s}$. The experimental apparatus is composed by a straight tube which has a length of 91.44 cm and an internal diameter of 8.51 mm, and is electrically heated (the nominal heat flux is 2.35 $\mathrm{MW/m^2}$) in the last part of the tube while the first third of the tube is unheated in order to have a developed flow-field in the heated region [12]. The experimental results are measured in the heated part of the tube by means of surface thermocouples, pressure taps and voltage measurement devices. Computations are made of the 2D axisymmetric configuration enforcing the following inlet boundary conditions inferred from experimental data: static pressure $p_{in} = 5.0012$ MPa, density $\rho_{in} = 71.65$ $\mathrm{kg/m^2}$, velocity $u_{in} = 18.5045$ m/s and $v_{in} = 0$ m/s. These conditions provide the same values as in the experimental test of static temperature and static pressure at the first instrumented test section and mass flow rate. Moreover, zero heat flux has been imposed in the first part of the tube and a non-constant heat flux distribution in the remaining length, as reported in [12]. In fact, the measured heat flux is different than that theoretically enforced because of the dependence of the channel material electric resistance on temperature and because of heat conduction through channel walls. For the latter reason, the heat flux is non-zero also in the nominal unheated region and a linear interpolation has been assumed to enforce the smooth transition between the adiabatic and heated part of the channel.

The numerical results are compared with the experimental data in Fig. 2 in terms of wall temperature and bulk temperature. Note that the heat flux deterioration is showed by the large pick of wall temperature (see Fig. 2(a)) occurring at $x \simeq 50$ cm. As can be seen in Fig. 2(b), the bulk temperature behavior is very well reproduced by the

numerical simulation with a discrepancy smaller than 0.2%. Also computed bulk pressure, velocity and density (not shown here) fall in the range of experimental test results, as the maximum discrepancy is only 0.1% for pressure, 0.5% for the density and 0.6% for the velocity. The wall temperature (Fig. 2(a)) shows a larger discrepancy, which however remains smaller than 6%. These comparisons are very satisfactory. In fact, the data of [12] are affected by an estimated experimental error of 3% for the mass flow rate, 4% for the inlet fluid temperature and 1% for the fluid pressure. Moreover, because the value of material electric resistance is considered no better than 10% accurate, the same uncertainty affects the estimate of the heat flux as it is a function of the electric power supplied and the wall material resistance.

For the sake of completeness, the results presented in Fig. 2 are also compared with grid converged FNS simulations carried out for this test case in [20]. As seen in the foregoing section, there are differences between PNS and FNS results. However, if compared to experimental data, both results are included within the data uncertainty. In particular, a good agreement is found on the bulk properties, whereas there is a greater discrepancy in the evaluation of wall properties (see for instance the wall temperature in Fig. 2(a)). It is interesting to note that in this case PNS results are even closer to experimental data than FNS results. Although the extremely high resolution in the streamwise direction of PNS and the different way of enforcing inlet and outlet boundary conditions could provide a partial explanation, the greater closeness of PNS results to experimental data with respect to FNS should be considered as fortuitous. The overall result is, however, that both approaches can be used to reasonably predict the flows of interest, as confirmed by comparison with experimental data. Besides, the most important result for the objectives of the present study is that the PNS approach provides solutions close to FNS also in the case of turbulent heated flow of a near critical fluid.

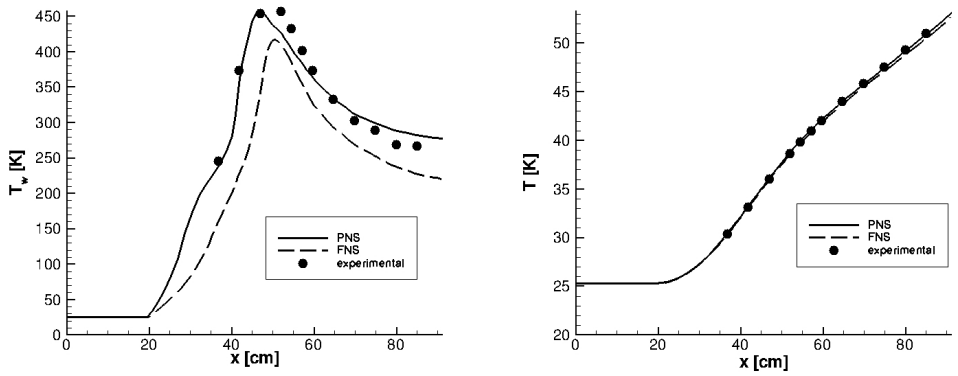

(a) wall temperature (b) bulk temperature

Figure 2: Comparisons between experimental data and numerical results

The good agreement between experimental data and numerical results on this test case proves therefore that the PNS solver could be a suitable tool to study complex thermodynamic phenomena, and among all the heat transfer deterioration, which is a phenomenon likely to occur in liquid rocket engine cooling channels.

6. Heated flow of supercritical methane

Besides to hydrogen, also methane channel flows have been considered so far. An example of a computation of heated methane flow is shortly described below to show the capability of handling numerically supercritical pressure methane. In particular, a simulation of supercritical methane flowing in a heated straight channel with a circular cross section has been carried out. The channel has a length of 200 diameters: therefore is long enough to have a developed flow. The boundary conditions are inferred to reproduce typical cooling channels conditions. In fact the flow is turbulent ($Re = 2.10^6$) and a constant heat load of $q_w = 10\,MW$ is applied along the channel. The pressure is supercritical ($p/p_c \simeq 2$) and the Mach number is $M \simeq 0.25$. The results are presented in Fig. 3-5. As can be seen in Fig 3 along the channel the expected velocity increase and density decrease is found, because of the wall friction and the heat flux. Also wall and bulk temperatures show the expected trend (Fig. 5): the bulk temperature always increases almost linearly because of the heat flux coming from the wall which is constant along the channel, whereas the wall

temperature increases with a changing trend along the channel because of the growth of the boundary layer.

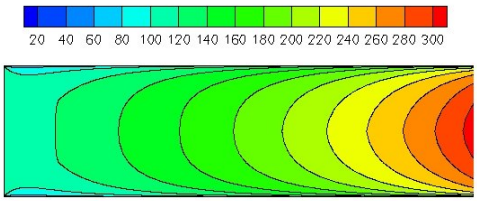

Figure 3: 2D stramwise velocity component field (m/s)

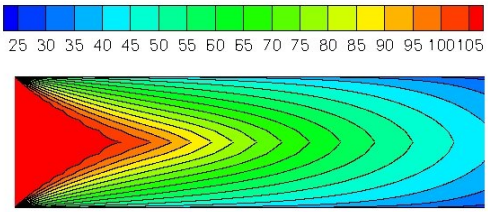

Figure 4: 2D density field (kg/m^2)

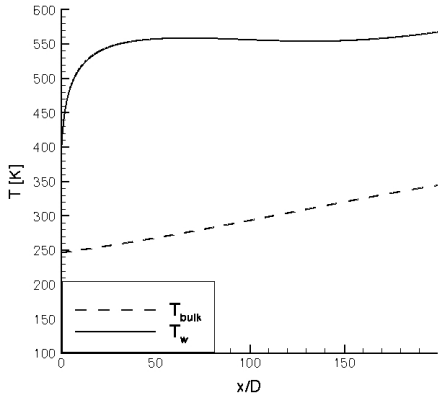

Figure 5: Bulk and wall temperature

Acknowledgments

Part of the presented study has been carried out within the project “In-Space Propulsion 1 program” granted from the European Comunity Seventh Framework program.

References

[1] Urbano, A. and Nasuti, F., “Numerical Analysis of Heated Channel Flows by a Space-Marching Finite-Volume Technique,” AIAA Paper 2010-4315, 2010, 10th AIAA/ASME Joint Thermophysics and Heat Transfer Conference, Chicago, Illinois, June 28-1, 2010.

[2] Urbano, A. and Nasuti, F., "Numerical Analysis of Heated Channel Flows by a Space-Marching Finite-Volume Technique," *Journal of Thermophysics and Heat Transfer*, in press.

[3] Kunz, O., R.Klimeck, W.Wagner, and M.Jaeschke, "The GERG-2004 Wide-Range Equation of State for Natural Gases and Other Mixtures," Tech. rep., GERG TM15, 2007.

[4] Huber, M. L., Laesecke, A., and Perkins, R. A., "Model for the Viscosity and Thermal Conductivity of Refrigerants, Including a New Correlation for the Viscosity of R134a," *Ind. Eng. Chem. Res. 2003*, Vol. 42, 2003, pp. 3163–3178.

[5] Klein, S. A., McLinden, M. O., and Laesecke, A., "An improved extended corresponding states method for estimation of viscosity of pure refrigerants and mixtures," *International Journal of Refrigeration*, Vol. 20, No. 3, 1997, pp. 208–217.

[6] Vigneron, Y., Rakich, J., and Tannehill, J., "Calculation of Supersonic Viscous Flow over Delta Wings with Sharp Subsonic Leading Edges," AIAA Paper 78-1137, 1978.

[7] Spalart, P. and Allmaras, S., "A One-Equation Turbulence Model for Aerodynamic Flow," *La Recherche Aerospatiale*, Vol. 1, 1994, pp. 5–21.

[8] Roe, P., "Approximate Riemann Solvers, Parameter Vectors, and Difference Schemes," *Journal of Computational Physics*, Vol. 43, 1981, pp. 357–372.

[9] McLinden, M. O., Klein, S. A., and Perkins, R. A., "An extended corresponding states model for the thermal conductivity of refrigerants and refrigerant mixtures," *International Journal of Refrigeration*, Vol. 23, 2000, pp. 43–63.

[10] Huber, M. and Ely, J., "Prediction of viscosity of refrigerants and refrigerant mixtures." *Fluid Phase Equilibria*, Vol. 80, 1992, pp. 239–248.

[11] Huber, M., Friend, D., and Ely, J., "Prediction of thermal conductivity of refrigerants and refrigerant mixtures." *Fluid Phase Equilibria*, Vol. 80, 1992, pp. 249–261.

[12] Hendricks, R., Graham, R., Hsu, Y., and Friedman, R., "Experimental Heat-Transfer Results for Cryogenic Hydrogen Flowing in Tubes at Subcritical and Supercritical Pressures to 800 Pounds per Square Inch Absolute," NASA TN D-3095, 1966.

[13] Sato, T., Sugiyama, M., Itoh, K., Mori, K., Fukunaga, T., Misawa, M., Otomo, T., and Takata, S., "Structural Difference Between Liquidlike and Gaslike Phases in Supercritical Fluid," *Physical Review E (Statistical, Nonlinear, and Soft Matter Physics)*, Vol. 78, No. 5, 2008, pp. 051503:1–9.

[14] Zhong, F., Fan, X., Yu, G., Li, J., and Sung, C., "Heat Transfer of Aviation Kerosene at Supercritical Conditions," *Journal of Thermophysics and Heat Transfer*, Vol. 23, No. 3, 2009, pp. 543–550.

[15] Koshizuka, S., N.Takano, and Oka, Y., "Numerical Analysis of Deterioration Phenomena in Heat Transfer to Supercritical Water," *International Journal of Heat and Mass Transfer*, Vol. 38, No. 16, 1995, pp. 3077–2084.

[16] Cheng, X., Kuang, B., and Yang, Y., "Numerical Analysis of Heat Transfer in Supercritical Water Cooled Flow Channels," *Nuclear Engineering and Design*, Vol. 237, No. 3, 2007, pp. 240–252.

[17] Shiralkar, B. and Griffith, P., "Deterioration in Heat Transfer to Fluids at Supercritical Pressure and High Heat Fluxes," *ASME Journal of Heat Transfer*, Vol. 91, No. 1, February 1968, pp. 27–36.

[18] Graham, R., Hendricks, R., and Simoneau, R., "Convective Heat Transfer to Low-Temperature Fluids," *Heat Transfer*, 1974.

[19] Wang, Y.-Z., Hua, Y.-X., and MengâĂă, H., "Numerical Studies of Supercritical Turbulent Convective Heat Transfer of Cryogenic-Propellant Methane," *Journal of Thermophysics and Heat Transfer*, Vol. 24, No. 3, 2010, pp. 490–500.

[20] Pizzarelli, M., Urbano, A., and Nasuti, F., "Numerical Analysis of Deterioration in Heat Transfer to Near-Critical Rocket Propellants," *Numerical Heat Transfer, Part A: Applications*, Vol. 57, 2010, pp. 297–314.